

High Precision Measurements of Interstellar Dispersion Measure with the upgraded GMRT

M. A. Krishnakumar^{1*}, P. K. Manoharan², Bhal Chandra Joshi³, Raghav Girgaonkar⁴, Shantanu Desai⁴, Manjari Bagchi^{5,6}, K. Nobleson⁷, Lankeswar Dey⁸, Abhimanyu Susobhanan⁸, Sai Chaitanya Susarla⁹, Mayuresh P. Surnis¹⁰, Yogesh Maan¹¹, A. Gopakumar⁸, Avishek Basu¹⁰, Neelam Dhanda Batra^{7,12}, Arpita Choudhary⁵, Kishalay De¹³, Yashwant Gupta³, Arun Kumar Naidu¹⁴, Dhruv Pathak^{5,6}, Jaikhomba Singha¹⁵, T. Prabu¹⁶

¹ Fakultät für Physik, Universität Bielefeld, Postfach 100131, 33501 Bielefeld, Germany

² Arecibo Observatory, University of Central Florida, Arecibo, PR 00612, USA

³ National Centre for Radio Astrophysics, Tata Institute of Fundamental Research, Ganeshkhind, Pune 411007, Maharashtra, India

⁴ Department of Physics, Indian Institute of Technology Hyderabad, Kandi, Telangana 502285, India

⁵ The Institute of Mathematical Sciences, C. I. T. Campus, Tharamani, Chennai 600113, Tamil Nadu, India

⁶ Homi Bhabha National Institute, Training School Complex, Anushakti Nagar, Mumbai 400094, Maharashtra, India

⁷ Department of Physics, BITS Pilani Hyderabad Campus, Hyderabad 500078, Telangana, India

⁸ Department of Astronomy and Astrophysics, Tata Institute of Fundamental Research, Dr. Homi Bhabha Road, Mumbai 400005, Maharashtra, India

⁹ Indian Institute of Science Education and Research Thiruvananthapuram, Vithura, Kerala 695551, India

¹⁰ Jodrell Bank Centre for Astrophysics, University of Manchester, Oxford Road, Manchester, M13 9PL, UK

¹¹ ASTRON, the Netherlands Institute for Radio Astronomy, Postbus 2, 7990 AA, Dwingeloo, The Netherlands

¹² Department of Physics, Indian Institute of Technology Delhi, New Delhi-110016, India

¹³ Cahill Center for Astrophysics, California Institute of Technology, 1200 E. California Blvd. Pasadena, CA 91125, USA

¹⁴ University of Oxford, Sub-Department of Astrophysics, Denys Wilkinson Building, Keble Road, Oxford, OX1 3RH, United Kingdom

¹⁵ Department of Physics, Indian Institute of Technology Roorkee, Roorkee 247667, Uttarakhand, India

¹⁶ Raman Research Institute, Bengaluru 560080, Karnataka, India

Received XXX XX, XXXX; accepted YYY YY, YYYY

ABSTRACT

Context. Pulsar radio emission undergoes dispersion due to the presence of free electrons in the interstellar medium (ISM). The dispersive delay in the arrival time of pulsar signal changes over time due to the varying ISM electron column density along the line of sight. Correcting for this delay accurately is crucial for the detection of nanohertz gravitational waves using Pulsar Timing Arrays. **Aims.** We aim to demonstrate the precision in the measurement of dispersion delay achieved by combining 400–500 MHz (*BAND3*) wide-band data with those at 1360–1460 MHz (*BAND5*) observed using the upgraded GMRT, employing two different template alignment methods.

Methods. To estimate the high precision dispersion measure (DM), we measure high precision times-of-arrival (ToA) of pulses using carefully generated templates and the currently available pulsar timing techniques. We use two different methods for aligning the templates across frequency to obtain ToAs over multiple sub-bands, and therefrom measure the DMs. We study the effects of these two different methods in detail on the measured DM values.

Results. We present in-band and inter-band DM estimates of four pulsars over the timescale of a year using two different template alignment methods. The DMs obtained using both these methods show only subtle differences for PSR J1713+0747 and J1909–3744. A considerable offset is seen in the DM of PSR J1939+2134 and J2145–0750 between the two methods. This could be due to the presence of scattering in the former and profile evolution in the latter. We find that both methods are useful but could have a systematic offset between the DMs obtained. Irrespective of the template alignment methods followed, the precision on the DMs obtained is about 10^{-3} pc cm⁻³ using only *BAND3* and 10^{-4} pc cm⁻³ after combining data from *BAND3* and *BAND5* of the uGMRT. In a particular result, we have detected a DM excess of about 5×10^{-3} pc cm⁻³ on 24 February 2019 for PSR J2145–0750. This excess appears to be due to the interaction region created by fast solar wind from a coronal hole and a coronal mass ejection (CME) observed from the Sun on that epoch. A detailed analysis of this interesting event is presented.

Key words. pulsars:general – ISM:general – Gravitational Waves – Sun:coronal mass ejections

1. Introduction

Pulsars are rotating neutron stars that emit broadband radiation received as pulsed signals by the observers. The pulsar radiation reaches the observer after propagating through the ionised inter-

stellar medium (IISM) which disperses the pulsed signal, thereby delaying the times of arrival (ToAs) of pulses as a function of the observing frequency (Lorimer & Kramer 2004). This dispersion delay is directly proportional to the integrated column density of free electrons in the IISM, usually referred to as the dispersion measure (DM), and inversely proportional to the square of the

* E-mail: kkma@physik.uni-bielefeld.de

observing frequency (ν). Precise measurements of the DM can therefore be made by measuring the pulse ToAs simultaneously at different observing frequencies (e.g. [Backer 1996](#); [Ahuja et al. 2005, 2007](#)).

The DM of a pulsar can vary with time due a number of reasons that include the relative motion of the pulsar with respect to the observer, solar wind, terrestrial ionosphere, and the dynamical nature of the IISM. Typical DM variations observed in pulsars range from $10^{-3} - 10^{-4}$ pc cm $^{-3}$ ([Kumar et al. 2013](#); [Alam et al. 2020](#); [Donner et al. 2020](#)). If these variations are not accounted for, systematic errors of the order of $1 \mu\text{s}$ or more can arise while correcting for the DM delay to generate infinite-frequency ToAs in the solar system barycentre (SSB) frame ([Hobbs et al. 2006](#); [Edwards et al. 2006](#)). Such unaccounted systematics have the potential to degrade the ability of millisecond pulsars (MSP) to act as very accurate celestial clocks ([Hobbs et al. 2019](#)). The technique of pulsar timing that creates such celestial clocks requires us to model and characterize correctly the pulse propagation effects ([Edwards et al. 2006](#)). This technique is crucial for the rapidly maturing Pulsar Timing Array (PTA) efforts to detect nanohertz gravitational waves ([Foster & Backer 1990](#); [Arzoumanian et al. 2020](#)). PTAs pursue timing of tens of MSPs to detect mainly a stochastic nanohertz gravitational wave background due to an ensemble of merging supermassive black hole binaries ([Burke-Spolaor et al. 2019](#)).

There are three established PTA efforts and they are the Parkes Pulsar Timing Array (PPTA: [Hobbs 2013](#); [Kerr et al. 2020](#)), the European Pulsar Timing Array ([Kramer & Champion 2013](#); [Desvignes et al. 2016](#)), and the North American Nanohertz Observatory for Gravitational Waves (NANOGrav: [McLaughlin 2013](#); [Alam et al. 2020](#)). In addition, PTA efforts are gathering pace in India under the auspices of the Indian Pulsar Timing Array (InPTA: [Joshi et al. 2018](#)). The International Pulsar Timing Array (IPTA) consortium combines data and resources from various PTA efforts to enable faster detection of nanohertz GWs ([Perera et al. 2019](#)). It should be noted that high precision DM measurements are essential for reaching the desired sensitivities of existing PTAs as precise pulse ToA estimates depend on accurate DM measurements. While PPTA mostly relies on data above 800 MHz, NANOGrav uses narrow band (25–50 MHz) low frequency observations (430 MHz), in addition to the high frequency observations (1.4 GHz and above) in their campaign. On the other hand, InPTA covers the low frequencies with wide-band receivers, where the dispersion is most prominent. This allows precision in-band DM estimates (for example, see [Liu et al. 2014](#)). When combined with simultaneous higher frequency observations, high precision DM estimates are possible. In this paper, we assess the usefulness of this combination for high precision DM measurements.

It is therefore of utmost importance to such experiments that the pulsar DMs are measured to high precision. As the DM delay scales with the observing frequency as $\Delta_{\text{DM}} \propto \text{DM} \nu^{-2}$, high precision DM measurements are possible at lower observing frequencies, although one must be mindful of certain caveats such as the frequency dependence of DM due to multi-path propagation through the IISM ([Cordes et al. 2016](#); [Donner et al. 2019](#)) as well as the effect of variable scatter broadening of the pulse profiles observed at low radio frequencies while applying low frequency DM measurements to correct ToAs measured at high frequencies.

With the advent of a new-generation of upgraded telescopes and their wide-band receivers, the attainable precision in DM measurements has greatly improved in recent years (e.g. [Kaur et al. 2019](#); [Tiburzi et al. 2019](#); [Donner et al. 2020](#)). The Giant

Metre-wave Radio Telescope (GMRT: [Swarup et al. 1991](#)) has recently gone through a major upgrade of its receivers and back-end instrumentation (uGMRT: [Gupta et al. 2017](#); [Reddy et al. 2017](#)), which has enabled an almost seamless frequency coverage from 120 to 1450 MHz. This improvement in the frequency coverage along with its capability of simultaneously observing a source at different frequency bands using multiple subarrays has greatly enhanced the precision with which the uGMRT can measure pulsar DMs. This enables uGMRT to play an important role in eliminating low frequency DM noise in PTA experiments.

In our technique, we use multiple profiles obtained across wide bandwidths for DM estimation. The DM obtained with this method will be insensitive to profile evolution over frequencies as the model template will also be similarly frequency resolved. One important factor in getting the correct DM is the alignment of the sub-band profiles in the template. Small differences in the alignment can cause a systematic offset in the measured DM, and will make it difficult to combine with other PTA datasets or to apply at higher frequencies. In this paper, we discuss two different ways of aligning the wide-band profiles to measure in-band (*BAND3* alone) and inter-band (*BAND3* and *BAND5* combined) DMs using data obtained by the uGMRT (details of the band definitions can be found in Section 2).

The four pulsars for which we present our initial analysis are PSRs J1713+0747, J1909–3744, J1939+2134 and J2145–0750. Amongst these, PSR J2145–0750 has low solar elongations between December to February every year. This implies that DM for this pulsar has excess contribution from solar wind every year when it is close to the Sun ([Kumar et al. 2013](#); [Tiburzi et al. 2019, 2020](#); [Alam et al. 2020](#); [Donner et al. 2020](#)). DM can also be enhanced in case of a violent solar event, such as a coronal mass ejection (CME) or a CME-solar wind or CME-CME interaction, where the electron density in the line of sight can get enhanced. We report on such a DM excess event for the first time observed in our data.

The plan of the paper is as follows. The details of our observations are presented in Section 2. Our DM estimation methods are described in Section 3, followed by results on individual pulsars in Section 4. We compare the precision in DM that we can achieve with the uGMRT with other PTAs and discuss our results in Section 5.

2. Observation and data processing

In this work, we use observations of four MSPs conducted between April 2018 and March 2019 as part of the InPTA campaign. PSRs J1713+0747, J1909–3744 and J1939+2134 were chosen for this study due to their significant long-term DM variations ([Alam et al. 2020](#); [Donner et al. 2020](#)), while PSR J2145–0750 was chosen due to its high brightness for in-band analysis. Moreover, J1713+0747 and J1909–3744 are two pulsars with the highest timing precision achieved in PTA experiments ([Verbiest et al. 2016](#); [Alam et al. 2020](#)).

The pulsars were observed typically once every two weeks using the uGMRT in a multi-band phased array configuration. The 30 antennas of the uGMRT were split into three phased subarrays with the innermost 5 antennas used in *BAND3* (400–500 MHz), 12 of the remaining outer antennas used in *BAND5* (1360–1460 MHz), and another 8 used in *BAND4* (650–750 MHz). Each pulsar was observed in the three bands *simultaneously* at every epoch. The data in each band were acquired using a 100 MHz band-pass with 1024 sub-bands, where *BAND3* and *BAND5* data were coherently dedispersed using a real-time coherent dedispersion pipeline ([De & Gupta 2016](#)) to the known

Table 1: Summary of the observations used in this work. The table lists the duration of a single observation, the median signal to noise (S/N) ratio obtained in *BAND3* and *BAND5* after removing the non-detections, and the total number of observations for each pulsar. The observations were carried out over a time period from April 2018 to March 2019.

| PSR | Observation duration (mins) | Median S/N | | No. of Epochs |
|------------|-----------------------------|--------------|--------------|---------------|
| | | <i>BAND3</i> | <i>BAND5</i> | |
| J1713+0747 | 20 – 25 | 40 | 50 | 17 |
| J1909–3744 | 20 – 30 | 30 | 20 | 20 |
| J1939+2134 | 10 – 15 | 250 | 70 | 20 |
| J2145–0750 | 10 – 25 | 230 | 60 | 17 |

DM of the pulsar. The coherently dedispersed data were sampled at $81.92 \mu\text{s}$ sampling time and recorded for further processing. In this work, we only used the coherently dedispersed data obtained with *BAND3* and *BAND5*, as the incoherently dedispersed *BAND4* data were of much lower sensitivity for the in-band analysis described later. Further details on the available uGMRT configurations may be found in Gupta et al. (2017) and Reddy et al. (2017).

The timing mode data generated by the uGMRT were recorded using the GMRT Wide-band Backend (GWB: Reddy et al. 2017) in a raw data format without any metadata, which requires preprocessing before it can be analysed by widely used pulsar software such as PSRCHIVE (Hotan et al. 2004). We convert this raw data to the Timer format (van Straten & Bailes 2011) using a pipeline named `pinta`¹ (Susobhanan et al. 2020) developed for the InPTA campaign. `pinta` performs radio frequency interference (RFI) mitigation using either `gptool` (Chowdhury & Gupta 2021) or `RFIClean`² (Maan et al. 2020), and folds the data using `DSPSR` (van Straten & Bailes 2011), while supplying the required metadata (such as observing frequency and bandwidth) based on the observatory settings under which the observation was carried out. We supplied `DSPSR` with the pulsar models available from the IPTA Data Release 1 (Verbiest et al. 2016) for folding. In the analysis presented in this work, we exclusively use `RFIClean` for RFI mitigation, which is designed to remove periodic RFI such as the RFI caused by the 50 Hz power distribution grid as well as narrow band and spiky RFI.

The details of the observations and the achieved profile signal-to-noise (S/N) ratios over the entire band are summarized in Table 1. Both in-band and inter-band estimates of the DM are presented in this work, which required reasonably high S/N (> 30) within individual sub-bands, and this was achieved on most epochs. A plot of the frequency evolution of the four pulsars used in this work and their integrated profiles at both the bands are shown in Figure 1. Multiple high S/N ratio observations were added together to obtain the data plotted in this figure.

3. Data Analysis

The data folded with `DSPSR` after removing the RFIs using `RFIClean` are directly used for estimating the DM. Due to the limited time span of the dataset (~ 1 year), it is not possible to obtain a reliable timing solution from these data. Hence, we used the latest parameter files published by the NANOGrav collaboration in their 12.5 year data release (Alam et al. 2020) for esti-

imating DM. The first requirement for obtaining a high precision DM measurement using a wide-band data like ours is to obtain a frequency resolved high S/N ratio template and aligning the sub-band profiles properly so that there is no residual DM delay in the template. If this correction is not done properly, the DMs estimated using such a template will be biased. We have used two different methods to align the sub-band profiles in the template to check their effectiveness on the DM measurements as described in Section 3.1 below. We used these frequency resolved templates to obtain ToAs and measure DM using `TEMPO2` (Hobbs et al. 2006). A python based script was developed for this purpose using the PSRCHIVE tools. We have also implemented an outlier rejection algorithm for removing large outlier ToAs using Huber Regression (Huber 1964) following Tiburzi et al. (2019). Details of our DM measurements are given in Section 3.2.

3.1. Selection of the template and their alignment

In our first method (`METHOD1`), we selected an epoch where the S/N ratio of the observation is comparatively high at both bands (*BAND3* and *BAND5*). We estimated the DM at *BAND3* using the `pdmp` program available with PSRCHIVE. Although the precision with which `pdmp` reports the DM is not very high, it is sufficient to align the sub-band profiles well in most cases. If the precision in the DM measurement reported by `pdmp` is worse than the change in DM from the ephemeris (with which the data is dedispersed), we did not update the DM (This is the case with PSR J1909–3744). The obtained DM is then used to dedisperse both the *BAND3* and *BAND5* data. Smoothed templates were created from these files with the `psrsmooth` program in PSRCHIVE using the wavelet smoothing algorithm (Demorest et al. 2013). These smoothed templates were later used to estimate the DM.

It is possible that `METHOD1` could bias the DM measurements as the alignment of the templates is performed using `pdmp` DM, which tries to maximise the S/N ratio while obtaining the best DM. To circumvent this issue, we employed a different method (`METHOD2`) for alignment using an analytic template derived from the data. To do this, we added some of the high S/N ratio observations at both the bands to create high S/N ratio data. A frequency and time averaged profile was produced from these data at *BAND3*. We used the PSRCHIVE tool `paas` to create an analytic template by fitting multiple Gaussian functions to this profile. The noise-free template created with the best fit obtained with `paas` was then used to estimate the DM of the high S/N ratio *BAND3* data we have produced above using the method explained in section 3.2. The sub-band profiles in the high S/N ratio data were then aligned using this DM for both the bands. We then used `psrsmooth` as in the previous case to obtain noise free frequency resolved template. The frequency resolved templates produced using both the methods described above were then used to obtain the DM time series as described in the following section.

The DMs obtained using `METHOD2` have, in general, an order of magnitude better uncertainties than the ones obtained with `METHOD1`. We also note that, in some cases, the actual DM value obtained using the two methods were slightly different. Additionally, it is possible for `METHOD2` to give a biased DM for pulsars that show significant profile component evolution within the band as the initial alignment is obtained using a frequency averaged profile.

¹ <https://github.com/abhisrkckl/pinta>

² <https://github.com/ymaan4/rficlean>

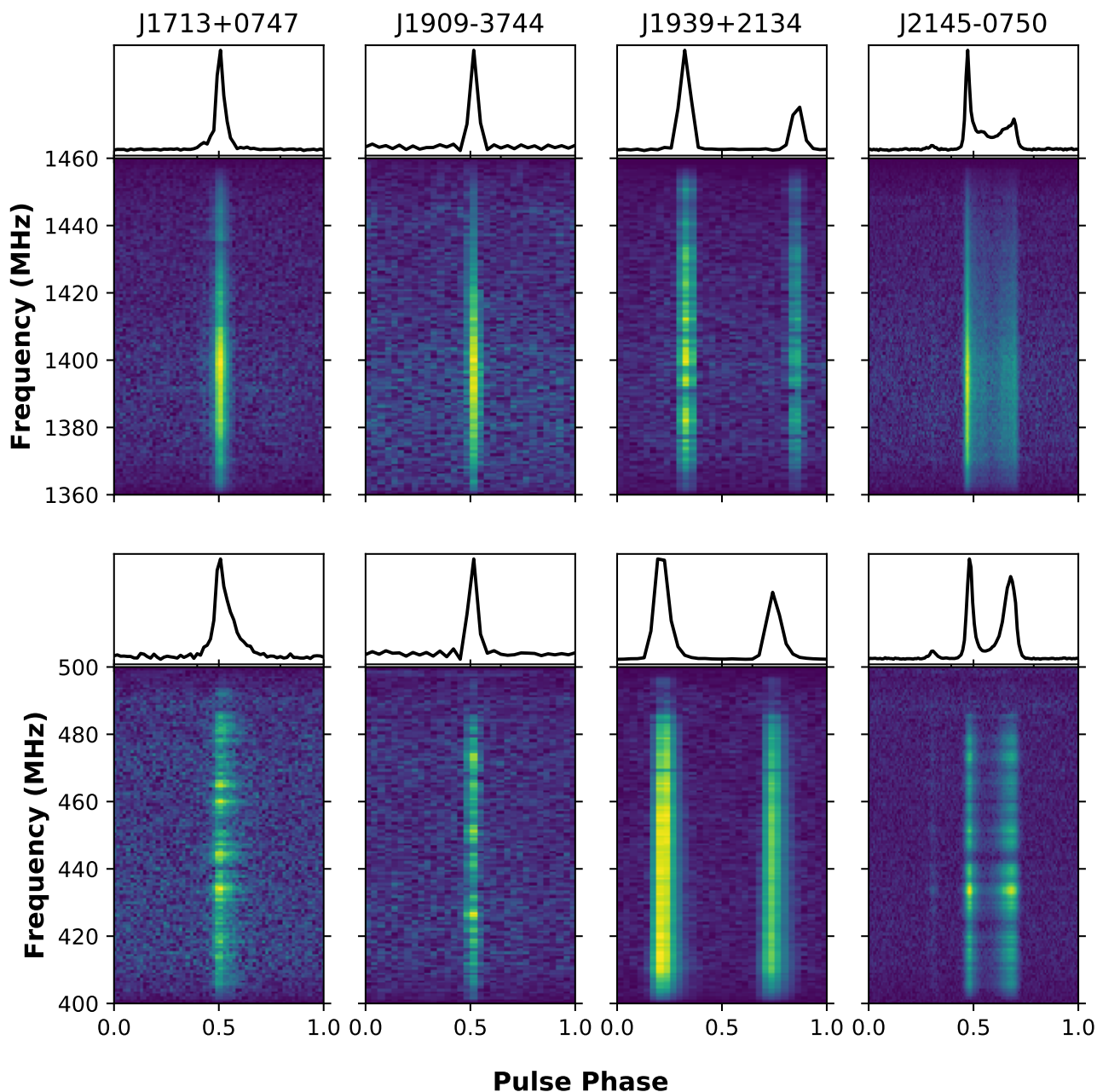


Fig. 1: A collage of the frequency evolution seen in the pulse profiles of the four pulsars presented in this work, along with their frequency averaged profiles. Top panel shows the data from *BAND5* and bottom panel shows *BAND3* data. The data for the plot was obtained after adding multiple observations together using the known ephemeris of each pulsar.

3.2. Measurement of DM

To measure the DM, we have used frequency resolved templates prepared as explained in Section 3.1. This approach removes the need of fitting other frequency dependent parameters while fitting for DM as the pulsar profile shape at a given frequency remains very much invariant (except for mode changes or scattering variations). The DMs reported in this paper are obtained using the TEMPO2 package. We have made use of the python inter-

face of PSRCHIVE for obtaining the ToAs and also for removing the outliers. Most of the data processing was performed with this Python interface except for obtaining the ToA residuals and for fitting DM which were performed using TEMPO2. The procedure for performing the outlier rejection we use here closely follows that by Tiburzi et al. (2019). A Python based tool, DMcalc was developed for performing the above operations.

**Source: PSR J2145-0750; MJD: 58538.2306; Prefit Wrms: 17.71 μs ; Postfit Wrms: 6.35 μs
 Median ToA Err: 7.31 μs ; DM: 9.010648 \pm 0.000578 pc cm^{-3} ; Reduced χ^2 : 0.50**

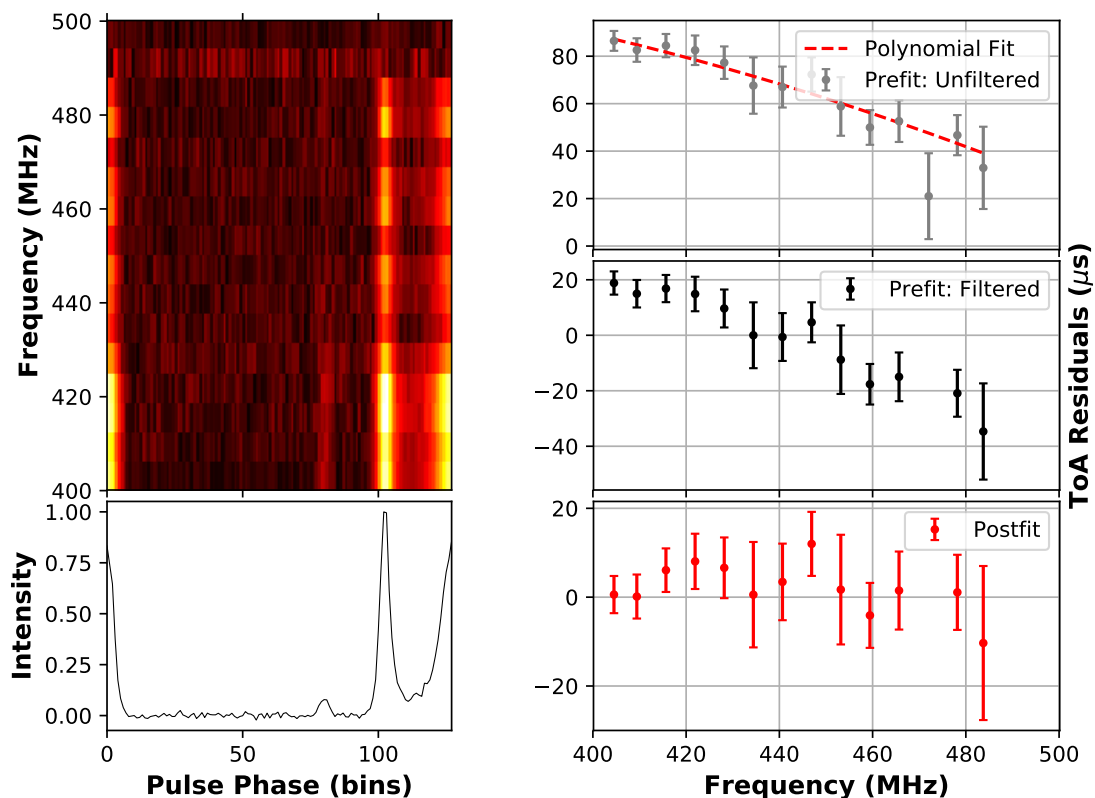


Fig. 2: A sample analysis plot of `DMcalc` using the observation of PSR J2145–0750 at *BAND3* on 24 February 2019, when an excess DM was seen towards this pulsar (See Section 4 for the discussion). Details of the fit can be found at the top of the plot. **Right panel:** The top plot shows the pre-fit residuals obtained from `TEMPO2` as gray circles and the Huber Regression fit to it as dashed line in red. The middle panel shows the prefit ToAs after removing the outliers. The bottom panel shows the ToAs after fitting for DM using `TEMPO2`. The details of the analysis method can be found in Section 3.2. **Left panel:** The top panel shows an image of the frequency spectra of the pulse profiles of a 25 min observation after applying the DM correction and the bottom shows the frequency and time averaged profile of the observation.

We used the latest parameter files published by Alam et al. (2020) for obtaining the DM. We have removed the DM and the DMX parameters from the parameter files as this could otherwise bias the measured DM values. FD parameters were also removed as we perform frequency resolved ToA estimation in this work. We have also kept the electron density due to the solar wind (`NE_SW`) as zero so as to not get biased with this value. The DM in the parameter file was updated to the one that is obtained using either `METHOD1` or `METHOD2` for use in both the methods. The ToAs with the given frequency resolution for each pulsar were obtained at both the bands by using the `ArrivalTime` class of `PSRCHIVE` available with the Python interface. We used the classical Fourier phase shift estimation method (Taylor 1992) implemented in `PSRCHIVE` as `PGS` for obtaining the ToAs. The ToAs thus obtained were then used to obtain frequency resolved timing residuals using the `general2` plugin of `TEMPO2`. A fit of ν^{-2} , where ν is the barycentric frequency of the ToAs was performed to these residuals using Huber Regression (Huber 1964). A robust median absolute deviation (MAD) of the ToA residuals after removing the above fit from the residuals is calculated and the ToAs beyond three times the MAD value on both sides of the ToA residuals were removed. This outlier rejection method is effective in removing the large

outliers which are otherwise present due to RFI or other issues in the data (for example, scintillation will make data of some channels almost unusable due to very low S/N ratio), which will corrupt the DMs obtained. These filtered ToAs were then used to fit for DM with `TEMPO2`.

An example analysis plot of PSR J2145–0750 is shown in Figure 2. In this particular fit, we used a total of 16 sub-band profiles across the available 100 MHz bandwidth. The top two sub-bands were removed from the template as they were contaminated by RFI at most of the epochs. A total of 14 ToAs were obtained out of which one was rejected based on the outlier rejection criteria discussed above. A fit for DM was performed and the resulting ToAs after removing the DM trend can be found at the bottom-right panel of the figure. The prefit and postfit weighted RMS can be found at the top of the panel, in addition to other parameters. As can be seen from the figure, the weighted RMS improved after fitting for DM and its value is close to the median ToA uncertainty.

This process is performed at *BAND3* and *BAND5* separately as well as in a combined *BAND3* + *BAND5* mode to obtain DMs. The addition of the data (or ToAs) without the requirement of having any jumps between the two bands is justified as these were observed simultaneously and processed with the

same pipelines, where the relative delay was experimentally determined to be zero (Susobhanan et al. 2020). The procedure was then repeated for all the observations to obtain the DM time series as shown in the Figure 3. In the case of inter-band DM measurements, the data of both the bands were aligned using the pulsar ephemeris before obtaining the ToAs and DM.

The four pulsars presented in this work have different frequency evolution of their parameters like flux density, profile shapes, scintille sizes and scatter broadening. To illustrate this, frequency resolved profiles for all the four pulsars are shown in Figure 1. As a result, we had to obtain ToAs with different frequency resolution for each of them as described in Section 4.

4. Results & Discussions

The DM time series obtained using the methods described in Section 4 for the four pulsars are shown in Figure 3. The left panel shows the DM measured using METHOD1 and the right panel shows DM obtained using METHOD2. The median DM values and their uncertainties for the four pulsars are listed in Table 2. We have only reported the measurements for which a reduced $\chi^2 < 10$ is obtained with TEMPO2. Some epochs show reduced χ^2 values worse than 10, but looking at each of them individually showed that they were affected by heavy RFI. Although we put a higher limit on χ^2 for getting the good measurements, most of them have reduced χ^2 much less than 10 and close to 1. The median value of the DMs estimated using METHOD1 and METHOD2 differs slightly for PSRs J1713+0747 and J1909–3744, while there is a clear offset between the DMs for PSRs J1939+2134 and J2145–0750. The possible cause of this difference is the underlying difference in the profile alignment methods used.

In the present work, we have used the data obtained by observing simultaneously at both *BAND3* and *BAND5* using a 100 MHz bandwidth. The fractional bandwidth at *BAND5* is a factor of ~ 4 – 5 smaller than those used by most of the other PTAs which reduces the precision with which we can obtain DM at *BAND5*. But a better fractional bandwidth at *BAND3* enables us to get a good handle on the DM. The DM precision we can obtain in general by using this dataset with the *BAND3* data alone is $\sim 10^{-3}$ and while combining the two bands it gets better by an order of magnitude to $\sim 10^{-4}$. In particular, we achieve an order of magnitude better precision of $\sim 10^{-4}$ with *BAND3* and 10^{-5} with *BAND3* and *BAND5* for PSR J1939+2134. Combining the two widely separated bands for measuring DM can create a bias due to the slightly different IISM the rays of these two bands pass through (Cordes et al. 2016).

Comparing our results obtained using the two methods described in this work to that of the recently published ones by Alam et al. (2020) and Donner et al. (2020) show interesting trends. For two pulsars, J1713+0747 and J2145–0750, we have data in both these datasets for comparison with ours. It should be noted that the data available from NANOGrav stops before our observations began whereas the data from Donner et al. (2020) covers this gap as well as extends beyond our dataset. For J1713+0747, we find our results from both methods to be consistent with the results from Donner et al. (2020), whereas it shows a small increase in DM of $\sim 2 \times 10^{-3}$ pc cm $^{-3}$ from NANOGrav results. For J2145–0750, the DM from METHOD1 shows a difference of $\sim 8 \times 10^{-3}$ pc cm $^{-3}$, whereas the ones obtained with METHOD2 show consistency with the other two datasets. For J1909–3744 and J1939+2134, we only have DM measurements from NANOGrav to compare, although the datasets do not overlap each other. For J1909–3744, the template DMs used for both

methods are different due to their inherent differences in obtaining it. A difference of $\sim 2 \times 10^{-3}$ pc cm $^{-3}$ in the DM applied in the template caused the difference in the obtained DM using our two methods. Both of these measurements will have a small bias if the NANOGrav DM time series is extrapolated to cover our epochs. For J1939+2134, both the alignment methods, METHOD1 as well as METHOD2, could create a bias due to scattering. A completely different method taking care of the scattering evolution for each observation has to be used in such a case, which will be taken up in a follow up work. In summary, both these alignment methods can be useful in getting DMs, but a systematic bias could be possible in either of the methods which will be very much pulsar specific. Below we discuss in detail the results of each of the pulsars studied in this paper.

4.1. PSR J1713+0747

This is one of the most precisely timed pulsars in PTA datasets. Apparently, the pulsar has so wide scintillation bandwidth at *BAND5* that at several epochs we could not detect the pulsar across the full 100 MHz bandwidth. This essentially reduced our DM precision at *BAND5* and also made some of the observations essentially unusable for our analysis. We collapsed the data to 16 channels at both the bands for obtaining the DMs. Both methods give similar DMs at both the bands, but the combined estimate shows a small bias. The DMs used for aligning the templates using both the methods are slightly different, by ~ 0.01 pc cm $^{-3}$. From Figure 3, it can be seen that the DM measurements at some epochs are missing in the left panel. This is because the reduced χ^2 of those fits are beyond the cutoff value and were removed from the plot. The average DM obtained in this work is consistent with that obtained by Donner et al. (2020) using LOFAR data, but is slightly higher than the DMs obtained by Alam et al. (2020) by about 2×10^{-3} pc cm $^{-3}$. This small bias from Alam et al. (2020) could be due to a frequency dependence of the DM (or scattering), as both *BAND3* and LOFAR frequency bands are close to each other. The median ToA precision obtained at *BAND5* is close to 1μ s.

4.2. PSR J1909–3744

Similar to the previous pulsar, this one is also a precisely timed pulsar with PTAs. Here also we collapsed the data to 16 channels at both the bands for DM measurement. The average DM obtained using the two methods, after combining the two bands show a slight difference. This small bias, as in the previous case, could be due to the initial DM used for aligning the templates (they differ by 3×10^{-3}). The pulse shape remains the same (without any major profile evolution) at both *BAND3* and *BAND5*. It is possible that we are unable to detect any small profile evolution due to the coarse sampling of the pulse phase. This prevented us from getting a better analytic profile for obtaining the DM with which the template was aligned. The DM time series reported in Alam et al. (2020) does not cover the epochs of our observations, but extrapolating their measurements to ours show a better alignment with the DMs obtained using METHOD1 and a small difference of $\sim 2 \times 10^{-3}$ pc cm $^{-3}$ with that of METHOD2, as evident from the difference in their average DMs. The ToA precision is similar at both the bands.

Table 2: Results. The table shows the ToA uncertainty for each pulsar when using frequency and time averaged profiles using the analytic template created with METHOD2 for both bands. The median DM and DM uncertainty obtained from the DM time series of each pulsar using METHOD1 and METHOD2 are also given.

| PSR | σ_{TOA} (μ s) | | DM [METHOD1] (pc cm^{-3}) | | | DM [METHOD2] (pc cm^{-3}) | | |
|------------|---------------------------|-------|--------------------------------------|-----------|-------------|--------------------------------------|-----------|-------------|
| | BAND3 | BAND5 | BAND3 | BAND5 | Combined | BAND3 | BAND5 | Combined |
| J1713+0747 | 3.2 | 1.2 | 15.991(2) | 15.99(2) | 15.9918(4) | 15.991(2) | 15.99(1) | 15.9900(2) |
| J1909-3744 | 2.1 | 2.1 | 10.389(2) | 10.46(6) | 10.3900(4) | 10.390(3) | 10.30(11) | 10.3878(5) |
| J1939+2134 | 0.9 | 0.4 | 71.01672(9) | 71.011(3) | 71.01661(3) | 71.02325(9) | 71.022(4) | 71.02267(5) |
| J2145-0750 | 1.7 | 3.7 | 8.995(1) | 8.95(9) | 8.9941(3) | 9.0048(7) | 9.00(8) | 9.0051(3) |

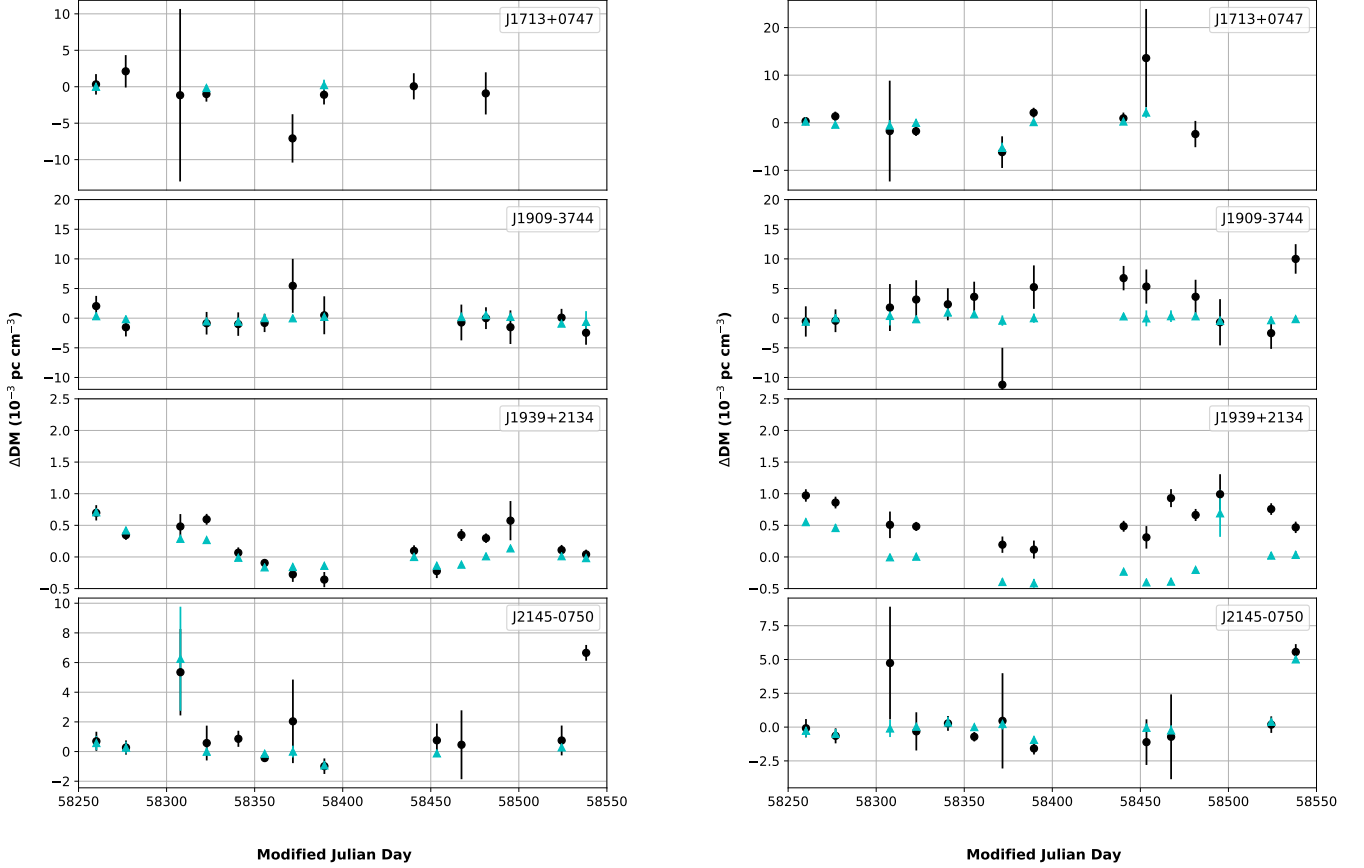


Fig. 3: The plots show the DM time series of the pulsars presented in this work. Left panel shows the DM time series obtained by METHOD1 and Right panel shows the DM time series obtained by METHOD2. Black filled circles represent DM obtained from BAND3 and Cyan triangles indicate DM obtained by combining bands 3 and 5. The median DM obtained from combining the two bands (Refer Table 2) are subtracted from the DM values to produce this plot. The DMs obtained with only using BAND5 data is not shown in the plot as their uncertainties are large.

4.3. PSR J1939+2134

This is one of the longest timed millisecond pulsar by all the PTAs (Kaspi et al. 1994; Verbiest et al. 2016). It shows timing noise in its ToA residuals and its timing data cannot be used for GW analysis without proper noise modeling. Since the pulsar is one of the brightest MSPs in our set, the precision in DM that can be achieved is quite high. Due to this, we used 128 channels at BAND3 and 32 channels at BAND5 in the DM analysis. One limitation this pulsar has for using the BAND3 data for es-

timating DM is that it has very strong scatter broadening. Due to this reason, the initial DM obtained by the two different methods we used differ by about $\sim 6 \times 10^{-3} \text{ pc cm}^{-3}$. This is exactly the difference between the average DMs reported in Table 2 for the combined bands. There is a small difference of $\sim 5 \times 10^{-4}$ between the BAND3 DMs and the combined ones obtained using METHOD2. This is probably due to the presence of scattering at BAND3. The DM obtained using both the methods show differences even after taking these biases into account. This indicates that the scatter broadening present in the pulsar signal is also

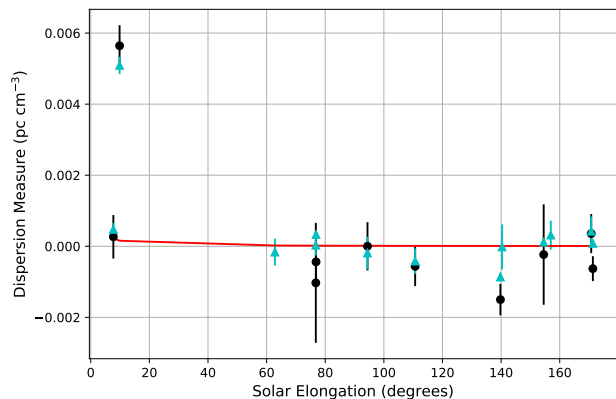


Fig. 4: The DM time series of PSR J2145–0750 plotted as a function of solar elongation. The colour scheme is the same as in Figure 3. The red line shows the expected DM excess by the solar wind as obtained from TEMPO2.

time varying. A proper analysis of scatter broadening and simultaneous measurement of DM is required to disentangle the DM getting biased by the extra delay caused by scattering. This will be taken up in a future study. The DM time series obtained using METHOD1 follows the trend seen in Alam et al. (2020), although the DMs reported here suffer from scattering bias. The ToA precision we obtain are the best for this pulsar in our sample, which is also indicative of the DM precision we could achieve.

4.4. PSR J2145–0750

This is one of the brightest pulsars in our sample. It shows strong profile evolution across both of the bands. Moreover, this pulsar’s line of sight passes close to the Sun at a solar elongation of ~ 5 degrees. It has been reported previously that the DM shows an increase due to the increase in the heliospheric electron density (solar wind) as its line of sight approaches close to the Sun (Kumar et al. 2013; Alam et al. 2020; Donner et al. 2020; Tiburzi et al. 2020). Since this pulsar has several scintilles in BAND3 data, we collapsed it to 16 channels to reduce the effect of scintillation. At BAND5, we used 8 channels across the band. The median DMs obtained using the two methods shown in Table 2 differ by about 1.1×10^{-2} pc cm $^{-3}$ for the combined bands. Even though the S/N ratio of the data used for generating the template was good, the precision in DM using METHOD1 is worse than the difference quoted above. This is possibly due to change in relative amplitudes of profile components with frequency, which increases uncertainty while maximising S/N in pdmp. This is not an issue for METHOD2 which obtained a precision in the fourth decimal place for the profile alignment using the analytic template. Although this creates a constant bias between the DM time series obtained using the two methods, the trend in it is not much affected as can be seen in Figure 3. The DMs obtained with METHOD2 show better alignment with the ones from Alam et al. (2020) and Donner et al. (2020), while the ones obtained with METHOD1 have an offset. The median ToA precision we could obtain is about $4 \mu\text{s}$ at BAND5.

Since the line of sight to this pulsar passes close to the Sun (between January – March), we compare the observed DM time series as a function of solar elongation (obtained from TEMPO2 as *solarangle* You et al. 2007) as shown in Figure 4. The red

curve in the figure shows the expected DM excess caused by the background solar wind as predicted by the model incorporated in TEMPO2. We have only two observations as the line of sight to the pulsar passed close to the Sun, respectively, at solar elongations ~ 5 and ~ 10 degrees. In Figure 4, it is seen that the DM measurement on 10 February 2019 (MJD: 58524) at a solar elongation of ~ 5 degrees shows nominal increase and it is consistent to the value expected from the model, whereas the other measurement at about 10 degrees (i.e., a radial distance of ~ 40 solar radii) away from the Sun on 24 February 2019 (MJD: 58538) shows a DM excess of about an order of magnitude higher than the model. The DMcalc fit for this excess DM observed is shown in the Figure 2. To find the cause of this excess DM, we carefully examined the various solar datasets and solar wind measurements available during this epoch.

The examination of solar images from the Solar Dynamic Observatory (SDO: Pesnell et al. 2012) revealed the onsets of two eruptions, i.e., coronal mass ejections (CMEs) at ~ 10 degrees west of the Sun’s center between 03 and 24 UT on 23 February 2019. The *ahead* spacecraft of the Solar TERrestrial RELations Observatory (STEREO-A: Kaiser et al. 2008) was located 99 degree east of the Sun-Earth line and it observed the above eruptions at about 20 degree behind the west limb of the Sun. Since these CMEs originated close to the disk center and were relatively narrow, they did not fill and show their expansion outside the field of view of the occulting disk of the coronagraph at the near-Earth spacecraft. In addition to these CMEs, the SDO images showed the presence of a large coronal hole ~ 30 degree wide, extending from the origin of the CME to the east nearly along the equatorial region of Sun. The high-speed streams from the coronal hole were likely to interact with the slow speed solar wind as well as CMEs.

Figure 5 shows the typical geometry of the line of sight to the pulsar with respect to the Sun, the possible propagation direction of CMEs, and slow solar wind along the Parker (Archimedean) spiral. The analysis of the interplanetary magnetic field and solar wind plasma from the OMNI datasets revealed an interplanetary shock at 07:35 UT on 27 February associated with the interaction between the slow- and high-speed solar wind streams. Figure 6 shows a 3-day period solar wind and interplanetary magnetic field measurements from 26 to 28 February 2019, obtained from the OMNI database³. From top to bottom, the figure shows the solar wind proton density, velocity, temperature, plasma beta (β), and the magnitude of interplanetary magnetic field. The arrival of the shock is indicated by a vertical dotted line. The average ambient solar wind speed of ~ 300 to 350 km/s, observed during the later half of February 2019, suggests that the interaction by the high-speed streams of speed ~ 600 to 650 km/s, would have been formed and developed well ahead of its arrival at the Earth. The shock was followed by an intense interaction region, which was more than an order of magnitude denser than the ambient solar wind as well as about a half day wide in time. In the interaction region, the magnetic field exhibited large intensity fluctuations and the plasma beta, which is the ratio between the gas and magnetic pressures, also showed a large peak. The temperature, density and velocity measurements after the interaction region showed clear characteristics of the streams from the coronal hole. The backward projection of the interaction region suggests that the interaction would have crossed the pulsar line of sight on 24 February around 2 to 8 UT.

In the case of the ambient solar wind, the density decay with the distance from the Sun can be considered to be R^{-2} , typical for

³ <https://omniweb.gsfc.nasa.gov>

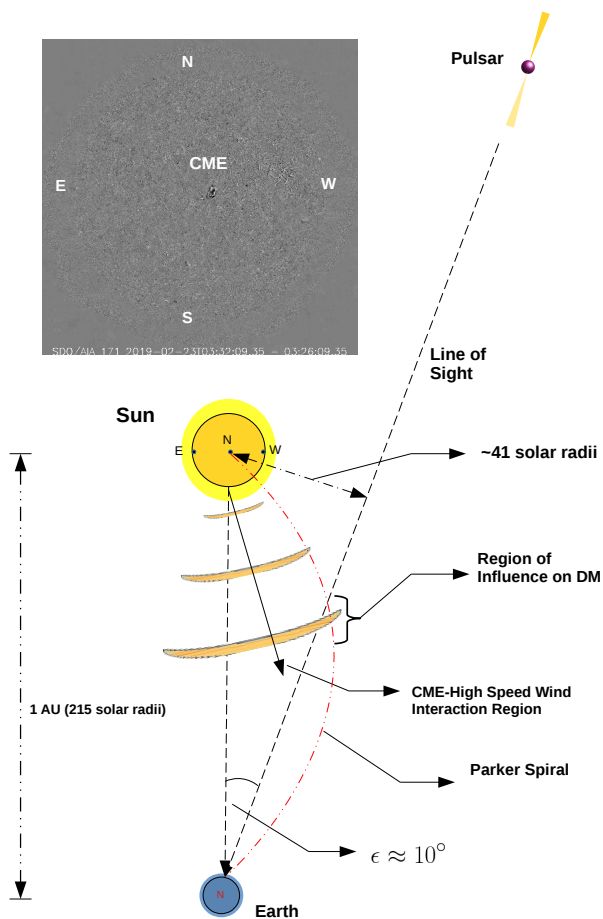


Fig. 5: A sketch showing the geometry of line of sight to the pulsar with respect to the Sun on 24 February 2019. The interaction region with excess electrons can be large in size while crossing the line of sight. The inset image shown at the top is the running difference EUV image of the Sun taken at 03:32 UT on 23 February 2019 by the SDO AIA telescope at 171 Å.

a spherically symmetric expansion of the solar wind, where R is the heliocentric distance. However, when the high density solar wind structures, such CMEs and/or high speed stream interactions are involved, a radial density gradient of $R^{-2.5}$ or steeper has been observed (e.g., Bird et al. 1994; Elliott et al. 2012).

Assuming the R^{-2} relation, it can be estimated that this interaction region had a density of $\sim 1 \times 10^3 \text{ cm}^{-3}$, taking 45 cm^{-3} as the density at Earth (1 AU). This density region (assuming the same extent of the interaction region at 41 solar radii) will create an excess DM of $1 \times 10^{-3} \text{ pc cm}^{-3}$. If we assume the steeper density gradient of $R^{-2.5}$, a DM excess of $3 \times 10^{-3} \text{ pc cm}^{-3}$ can be obtained. Another point to be considered is that the eastern side of the interaction region likely crossed the Earth and it was possibly a little less dense than the nose of the interaction region, as indicated by the *in situ* measurements. Thus, the excessive DM observed probably corresponds to the density enhancement caused by the interactions between high-speed and slow-speed solar wind and CMEs.

The solar wind stream interactions as well as stream-CME interactions are expected when the Sun is dominated by the mid-latitude and equatorial coronal holes. The vast sets of PTA and other pulsar observations available are likely to include many

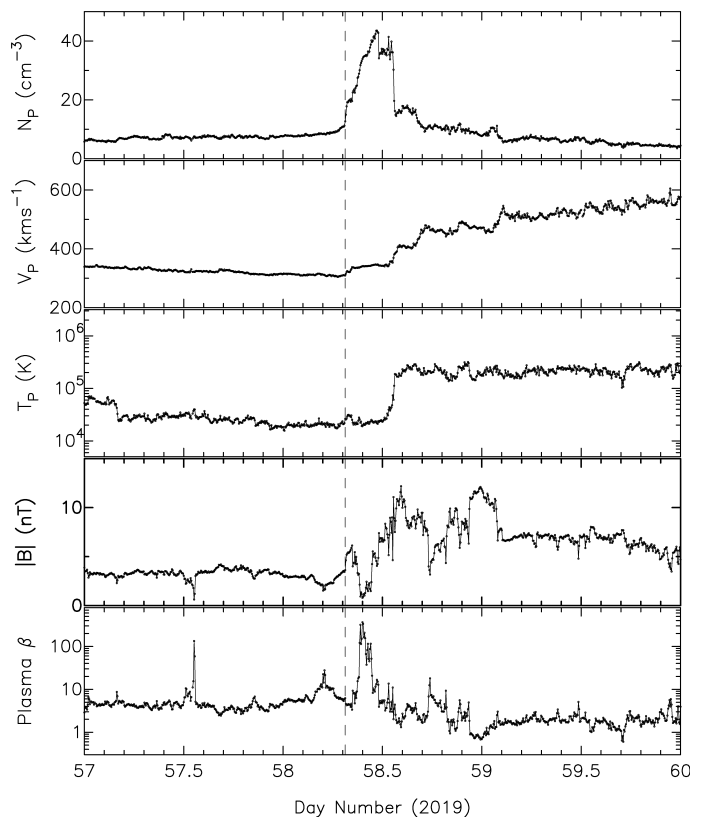


Fig. 6: *In situ* measured OMNI data for a 3-day period, from 26 to 28 February 2019, during the passage of interaction region associated with the high-speed solar wind streams and slow CME/ambient wind. From the top to bottom the following data are plotted: solar wind proton density (N_p), velocity (V_p), temperature (T_p), magnitude of the interplanetary magnetic field ($|B|$) and plasma beta (β). The vertical dashed line indicates the arrival of the interplanetary shock associated with the interaction region. The time immediately after the shock shows the intense interaction region, which is followed by the clear signatures of the high-speed streams from the coronal hole.

such events. A coordinated analysis of selected data sets would be of interest in understanding the effects of enhanced density structures of the solar wind on the DM variations as functions of solar offset and possibly also the phase of the solar cycle.

5. Summary & Conclusions

In this paper, we compared the two possible methods for aligning the frequency resolved pulsar profile templates and probed their effects on the resulting DM measurements. We used four InPTA pulsars observed by the uGMRT for a period of a year (two observing cycles at GMRT). These observations were done simultaneously at *BAND3* and *BAND5* of uGMRT with a 100 MHz bandwidth. For a uniform and systematic processing, we have developed a Python based tool, *DMcalc*, utilizing the *PSRCHIVE* Python interface and *TEMPO2* for estimating DM using the templates from the above two methods. We regularly obtained a DM precision of $\sim 10^{-3} \text{ pc cm}^{-3}$ at *BAND3* and $\sim 10^{-4} \text{ pc cm}^{-3}$ when combining it with *BAND5* data while using both of our template alignment methods.

We find that both the methods are useful for aligning the templates, but *METHOD2* could show a constant bias if the pulsar has scatter broadening. For pulsars that have no detectable

scatter broadening, the DMs obtained by METHOD1 show a consistent bias from that obtained with METHOD2. This is essentially due to the use of two different methods for template alignment. The METHOD1 uses an algorithm that aligns the multi-channel data by maximising the S/N ratio while the METHOD2 uses an analytic model derived from the frequency averaged profile of the data. We have compared the DMs obtained by these two methods with the other recently published results (Alam et al. 2020; Donner et al. 2020). Our DM measurements for PSRs J1713+0747 and J2145–0750 using METHOD2 compare very well with theirs, while those from METHOD1 show a bias. In the cases of PSRs J1909–3744 and J1939+2134, our data has no overlap with either of the published datasets. Nevertheless, we see a continuing trend of the NANOGrav DM time series for J1939+2134 using METHOD1, while METHOD2 shows a clear constant offset. An improved method that takes care of the scattering bias while estimating the DM will be able to remove any bias created by scattering. For J1909–3744, we expect to see a small offset from that of the NANOGrav data using both the methods, although the DMs obtained with METHOD1 may have smaller bias than the other.

We could obtain a ToA precision of $\sim 1\mu\text{s}$ or better for all the pulsars at both the bands, which is highly encouraging. We see the effect of scattering on DM measurements of J1939+2134. In a follow up study, we plan to disentangle the two effects to obtain better DM estimates.

We infer that the DM measurement at MJD 58538 of PSR J2145–0750 with a solar elongation of $\sim 10^\circ$ was enhanced by an interaction region formed by a CME and high speed solar wind from a coronal hole close to the origin of the CME. Similar events can be of interest to both the pulsar and the solar wind community and our results show that such studies can be pursued using high precision data from the uGMRT.

The present observations used a 20 – 25 mins scan for each pulsar. A much better precision on both ToAs and hence DM can be achieved by using longer integrations and wider bandwidths of the uGMRT. We have started doing observations using a bandwidth of 200 MHz at both BAND3 and BAND5 simultaneously and also increased the observation duration in addition to increasing the number of antennas at each band (by skipping BAND4, and utilizing the antennas at the other two bands). A factor of three improvement in the precision of DM is expected at BAND3 in general with this increased bandwidth as compared to current results. Initial results show vast improvement in the S/N ratio of the pulsars. The data from these observations are under various stages of processing and will be reported elsewhere.

Following the encouraging results from the work presented here, we plan to apply these techniques to our full sample of pulsars observed during the last four years. Additionally, efforts are being pursued for developing other methods to make the DM measurements even more precise and reliable, and therefore employable for the on-going gravitational wave analysis by the various PTAs.

Data Availability

The data used in this paper will be made available on reasonable request. The SDO 171Å images used for the solar wind analysis can be found at https://cdaw.gsfc.nasa.gov/movie/make_javamovie.php?date=20190223&img1=sdo_a304&img2=lasc2rdf The code used for measuring DM in this work, DMcalc is publicly available at <https://github.com/kkma89/dmcalc>.

Acknowledgements

MAK is thankful to Caterina Tiburzi and Joris Verbiest for their valuable inputs and useful discussions at various stages of this work. AS, AG, BCJ, LD, and YG acknowledge the support of the Department of Atomic Energy, Government of India, under project Identification # RTI 4002. BCJ, YG and AB acknowledge support from the Department of Atomic Energy, Government of India, under project # 12-R&D-TFR-5.02-0700. AC acknowledge support from the Women’s Scientist scheme (WOS-A), Department of Science & Technology, India. MPS acknowledges funding from the European Research Council (ERC) under the European Union’s Horizon 2020 research and innovation programme (grant agreement No. 694745). NDB acknowledge support from the Department of Science & Technology, Government of India, grant SR/WOS-A/PM-1031/2014. AB acknowledges the support from the UK Science and Technology Facilities Council (STFC). Pulsar research at Jodrell Bank Centre for Astrophysics and Jodrell Bank Observatory is supported by a consolidated grant from STFC. We thank the staff of the GMRT who made our observations possible. GMRT is run by the National Centre for Radio Astrophysics of the Tata Institute of Fundamental Research. The open data policy of STEREO and SDO teams is acknowledged. The solar wind and interplanetary data sets have been obtained from the OMNI database.

References

- Ahuja, A. L., Gupta, Y., Mitra, D., & Kembhavi, A. K. 2005, MNRAS, 357, 1013
Ahuja, A. L., Mitra, D., & Gupta, Y. 2007, MNRAS, 377, 677
Alam, M. F., Arzoumanian, Z., Baker, P. T., et al. 2020, arXiv e-prints, arXiv:2005.06495
Arzoumanian, Z., Baker, P. T., Blumer, H., et al. 2020, ApJ, 905, L34
Backer, D. C. 1996, in Compact Stars in Binaries, ed. J. van Paradijs, E. P. J. van den Heuvel, & E. Kuulkers, Vol. 165, 197
Bird, M. K., Volland, H., Paetzold, M., et al. 1994, ApJ, 426, 373
Burke-Spolaor, S., Taylor, S. R., Charisi, M., et al. 2019, Astronomy and Astrophysics Review, 27, 5
Chowdhury, A. & Gupta, Y. 2021, In preparation
Cordes, J. M., Shannon, R. M., & Stinebring, D. R. 2016, ApJ, 817, 16
De, K. & Gupta, Y. 2016, Experimental Astronomy, 41, 67
Demorest, P. B., Ferdman, R. D., Gonzalez, M. E., et al. 2013, ApJ, 762, 94
Desvignes, G., Caballero, R. N., Lentati, L., et al. 2016, Monthly Notices of the Royal Astronomical Society, 458, 3341
Donner, J. Y., Verbiest, J. P. W., Tiburzi, C., et al. 2020, arXiv e-prints, arXiv:2011.13742
Donner, J. Y., Verbiest, J. P. W., Tiburzi, C., et al. 2019, A&A, 624, A22
Edwards, R. T., Hobbs, G. B., & Manchester, R. N. 2006, Monthly Notices of the Royal Astronomical Society, 372, 1549
Elliott, H. A., Henney, C. J., McComas, D. J., Smith, C. W., & Vasquez, B. J. 2012, Journal of Geophysical Research (Space Physics), 117, A09102
Foster, R. S. & Backer, D. C. 1990, ApJ, 361, 300
Gupta, Y., Ajithkumar, B., Kale, H. S., et al. 2017, Current Science, 113, 707
Hobbs, G. 2013, Classical and Quantum Gravity, 30, 224007
Hobbs, G., Guo, L., Caballero, R. N., et al. 2019, Monthly Notices of the Royal Astronomical Society, 491, 5951
Hobbs, G. B., Edwards, R. T., & Manchester, R. N. 2006, Monthly Notices of the Royal Astronomical Society, 369, 655
Hotan, A. W., van Straten, W., & Manchester, R. N. 2004, Publications of the Astronomical Society of Australia, 21, 302–309
Huber, P. J. 1964, Ann. Math. Statist., 35, 73
Joshi, B. C., Arumugasamy, P., Bagchi, M., et al. 2018, Journal of Astrophysics and Astronomy, 39, 51
Kaiser, M. L., Kucera, T. A., Davila, J. M., et al. 2008, Space Sci. Rev., 136, 5
Kaspi, V. M., Taylor, J. H., & Ryba, M. F. 1994, ApJ, 428, 713
Kaur, D., Bhat, N. D. R., Tremblay, S. E., et al. 2019, ApJ, 882, 133
Kerr, M., Reardon, D. J., Hobbs, G., et al. 2020, Publications of the Astronomical Society of Australia, 37, e020
Kramer, M. & Champion, D. J. 2013, Classical and Quantum Gravity, 30, 224009
Kumar, U., Gupta, Y., van Straten, W., et al. 2013, in Neutron Stars and Pulsars: Challenges and Opportunities after 80 years, ed. J. van Leeuwen, Vol. 291, 432–434
Liu, K., Desvignes, G., Cognard, I., et al. 2014, MNRAS, 443, 3752

- Lorimer, D. & Kramer, M. 2004, Handbook of pulsar astronomy (Cambridge University Press)
- Maan, Y., van Leeuwen, J., & Vohl, D. 2020, arXiv e-prints, arXiv:2012.11630
- McLaughlin, M. A. 2013, Classical and Quantum Gravity, 30, 224008
- Perera, B. B., DeCesar, M. E., Demorest, P. B., et al. 2019, Monthly Notices of the Royal Astronomical Society, 490, 4666
- Pesnell, W. D., Thompson, B. J., & Chamberlin, P. C. 2012, Sol. Phys., 275, 3
- Reddy, S. H., Kudale, S., Gokhale, U., et al. 2017, Journal of Astronomical Instrumentation, 6, 1641011
- Susobhanan, A., Maan, Y., Joshi, B. C., et al. 2020, arXiv e-prints, arXiv:2007.02930
- Swarup, G., Ananthakrishnan, S., Kapahi, V. K., et al. 1991, Current Science, 60, 95
- Taylor, J. H. 1992, Philosophical Transactions of the Royal Society of London Series A, 341, 117
- Tiburzi, C., Shaifullah, G. M., Bassa, C. G., et al. 2020, arXiv e-prints, arXiv:2012.11726
- Tiburzi, C., Verbiest, J. P. W., Shaifullah, G. M., et al. 2019, MNRAS, 487, 394
- van Straten, W. & Bailes, M. 2011, PASA, 28, 1
- Verbiest, J. P. W., Lentati, L., Hobbs, G., et al. 2016, MNRAS, 458, 1267
- You, X. P., Hobbs, G. B., Coles, W. A., Manchester, R. N., & Han, J. L. 2007, ApJ, 671, 907